Penerbit Akademia Baru

Journal of Advanced Research in Fluid Mechanics and Thermal Sciences

Journal homepage: www.akademiabaru.com/arfmts.html
ISSN: 2289-7879

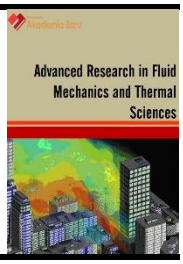

Aerodynamic Heating Distribution for Temperature Prediction of Fast Flying Body Nose Using CFD

Open Access

Emad Qasem Hussein[1], Farhan Lafta Rashid[1,*], Haider Nadhom Azziz[1]

[1] Department of Petroleum Engineering, University of Kerbala, Iraq

ARTICLE INFO

Article history:
Received 8 June 2019
Received in revised form 20 September 2019
Accepted 26 September 2019
Available online 28 December 2019

Keywords:
Aerodynamic heating; hypersonic flow; Fluent; dynamic mesh; attack angle

ABSTRACT

Aerodynamic heating has an important role on hypersonic flying bodies. The ANSYS Fluent 17.0 has been used in this study to investigate the aerodynamic heating and temperature predicted in an ogive and conical noses of a fly body. The results were compared for two noses of similar dimension, material and properties. Dynamic mesh must be used to simulate motion of the body nose at different attack angle and User Defined Function (UDF) is applied in the study to control the mesh deformation and to define its motion of body nose. The results presented herein are found that the magnitude of the internal heat distribution of temperature over the body nose is directly proportional with Mach number and attack angle. Moreover, as the attack angle increases, the heat distribution of temperature on the lower surface be much greater than it's on the upper surface. Finally, the heat distribution of temperature for a conical nose is higher than for an ogive nose about 3%. The obtained results in the present work are compared with analytical results to show the validation.

1. Introduction

A vehicle structures designed for hypersonic flights are subjected to severe aerodynamic heating during the lunch and re-entry phases of their operations [1]. Particles of air in the boundary layer closed to the body are affected by viscous or shearing, frictional forces. The particles velocity is reduced to zero at the surface. Therefore, the air particles kinetic energy within the boundary layer is converted to heat energy; this energy increases temperature of the boundary layer and skin of the body. It is well known that the excessive skin temperature can cause a failure of the structure or the control instrument imbedded inside the flying body. Consequently, all external surfaces on the vehicle are heated. The high heating associated with shocks at leading edges are significant issues in the vehicle design [2-3]. Drag and shock at the nose section will be generated from sudden compression to the incoming flow. The shock wave leads to make changes in the properties such as pressure, temperature, and velocity near the body surface. At high attach angle, the separation will be generated over a body which causes wake in the leeward side region [4].

* *Corresponding author.*
E-mail address: engfarhan71@gmail.com (Farhan Lafta Rashid)

In area of vehicle aerodynamics, it is more important to design optimum body nose shape, in order to get the streamline flow around the body to minimize the drag. The vehicle transports with high Mach numbers, thus skin friction and drag over the body is depend on its shape [5], Heat-absorbent material must therefore be provided to prevent destruction of the essential elements of the body structure. Thus, the amount of material added to keep the body nose from excessive aerodynamic heating must be minimized in order to keep the take-off weight to a practicable value [6].

In recent years, there have been significant investments in the development of fast vehicle technologies. Later extensive numerical analysis to obtain the temperature, heat transfer and pressure on steady and unsteady heat transfer in boundary layers of fast flow. Although some flight experiments are also conducted, to acquire aerodynamic heating data in the flight condition to evaluate these prediction methods [7]. Nassir *et al.,* [8] present the feasibility of vertical axis wind turbine potentiality to be placed along the highway's median in Malaysia. Rozaim *et al.,* [9] designed and fabricated the performance evaluation of low speed wind turbine.

The objective of the current study is to develop efficient engineering procedures for predicting the aerodynamic heating on a body nose configuration related to the Computational Fluid Dynamic (CFD) tools, the simulation is carried out using ANSYS program.

2. Physical Model

In this work, the flow field around spherical blunted nose shapes is investigated. In all of the following nose cone shape equations, L_0 is the overall length of the nose cone and R_0 is the radius of the base of the nose cone, *y* is the radius at any point *x*, as *x* varies from 0, at the tip of the nose cone, to L_0 .The geometry of these bodies was simplified in the numerical model as follows [10]:

2.1 Spherical Blunted Cone

A simple cone is very common nose shape. This cone is preferred for its simplicity of manufacture. The sides of a conical profile are straight lines:

$$y = \frac{xR_0}{L_0} \tag{1}$$

Cones are sometimes defined by their half angle φ

$$\varphi = \arctan\left(\frac{R_0}{L_0}\right) \quad and \quad y = xtan(\varphi) \tag{2}$$

In practical application, a conical nose is often blunted by capping it with a sphere segment, as shown in Figure 1. The tangency point where the sphere meets the cone can be expressed as;

$$x_t = \frac{L_0^2}{R_0}\sqrt{\frac{r_n^2}{R_0^2+L_0^2}} \tag{3}$$

$$y_t = \frac{x_t R_0}{L_0} \tag{4}$$

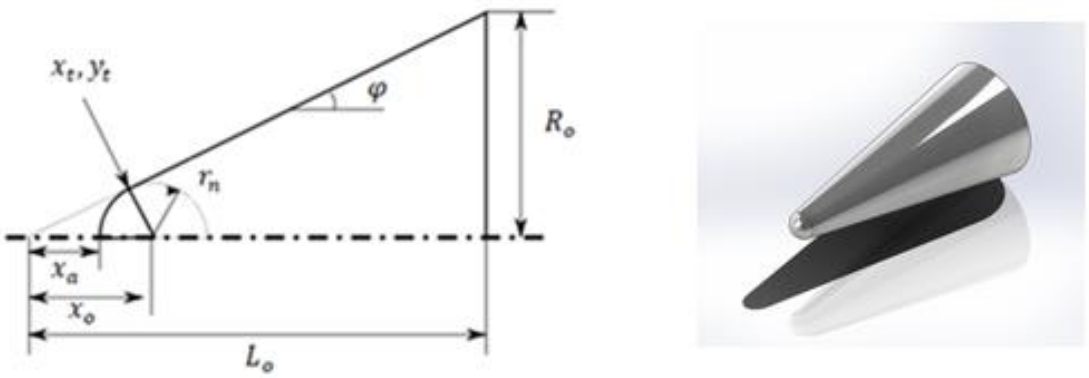

Fig. 1. Spherical blunted conic nose and profile with parameters [10]

The center of the spherical nose cap can be defined by

$$x_0 = x_t + \sqrt{r_n^2 - y_t^2} \tag{5}$$

And the apex point x_a can be found from:

$$x_a = x_0 - r_n \tag{6}$$

2.2 Spherical Blunted Tangent Ogive

The shape profile is formed by a circle segment like the vehicle body which tangents to the curves of the nose cone at the base. The vogue of this shape is largely due to the simplicity of constructing its profile, as shown in Figure 2.

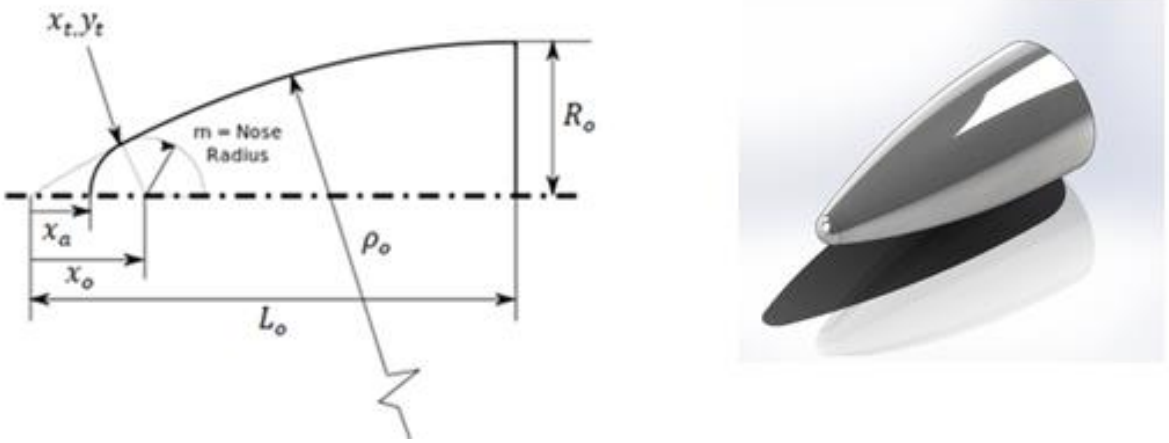

Fig. 2. Spherical blunted tangent ogive noise and profile with parameters [10]

The circle radius is known as the ogive radius, denoted by ρ_0 and it is regarded to the length and base radius of the nose cone as in the following relation

$$\rho_0 = \frac{R_0^2 + L_0^2}{2R_0} \tag{7}$$

The equation of the ogive segment in the x-y plane at any point x, as x varies from 0 to L_0 is

$$y = \sqrt{\rho_0{}^2 - (L_0 - x)^2} + R_0 - \rho_0 \quad (8)$$

A nose of tangent ogive is often weakened by capping it with a sphere segment. The point of tangency where the sphere meets the tangent ogive will be obtained from

$$x_0 = L_0 - \sqrt{(\rho_0 - r_n)^2 - (\rho_0 - R_0)^2} \quad (9)$$

$$y_t = \frac{r_n(\rho_0 - R_0)}{\rho_0 - r_n} \quad (10)$$

$$x_t = x_t + \sqrt{r_n^2 - y_t^2} \quad (11)$$

3. Methodology

The numerical simulation of 2-D heat transfer was performed by Fluent code. The CFD modelling includes numerical solution of the conservation equation for mass, momentum, and energy. The continuity equation can be written as follows [11-12].

$$\frac{\partial \rho}{\partial t} + \nabla.(\rho v) = 0 \quad (12)$$

The conservation of momentum is described by:

$$\frac{\partial}{\partial t}(\rho v) + \nabla.(\rho vv) = -\nabla P + \nabla.(\bar{\tau}) + \rho g + F \quad (13)$$

The stress tensor defined as follows

$$\tau = \mu\left((\nabla v + \nabla v^T) - \frac{2}{3}\nabla.vI\right) \quad (14)$$

where, I represents the unit tensor

The energy equation described by temperature can be written as follows

$$\rho c_p\left(\frac{\partial T}{\partial t} + v_x\frac{\partial t}{\partial x} + v_y\frac{\partial T}{\partial y} = \lambda\left(\frac{\partial^2 T}{\partial x^2} + \frac{\partial^2 T}{\partial y^2}\right)\right. \quad (15)$$

The specific dissipation rate ω and turbulence kinetic energy k can be obtained from the following transport equations [13].

$$\frac{\partial}{\partial t}(\rho k) + \frac{\partial}{\partial x}(\rho k v_x) + \frac{\partial}{\partial y}(\rho k v_y) = \frac{\partial}{\partial x}\left(\Gamma_k\frac{\partial \lambda}{\partial x}\right) + \frac{\partial}{\partial y}\left(\Gamma_k\frac{\partial \lambda}{\partial x}\right) + G_k - Y_k + S_k \quad (16)$$

$$\frac{\partial}{\partial t}(\rho \omega) + \frac{\partial}{\partial x}(\rho \omega v_x) + \frac{\partial}{\partial y}(\rho \omega v_y) = \frac{\partial}{\partial x}\left(\Gamma_\omega\frac{\partial k}{\partial x}\right) + \frac{\partial}{\partial y}\left(\Gamma_\omega\frac{\partial k}{\partial x}\right) + G_\omega - Y_\omega + S_\omega \quad (17)$$

The effective diffusivities for the $\kappa - \omega$ model can be expresses as

$$\left.\begin{aligned}\Gamma_k &= \mu + \frac{\mu_1}{\sigma_k} \\ \Gamma_k &= \mu + \frac{\mu_1}{\sigma_\omega}\end{aligned}\right\} \quad (18)$$

where, the terms G_k, Y_k represent the production and dissipation of turbulence kinetic energy, μ_1 is the turbulent viscosity and the terms G_ω, Y_ω represents the production and dissipation of specific dissipation rate.

4. Problem Specification

In an external flow such as that over a body nose, we have to define a far- filled boundary and mesh the region between the body nose geometry and boundary. The geometric model consists of C-type domain with radius (10) times length of body nose, which is located in the middle of domain as shown in Figure 3 [14].

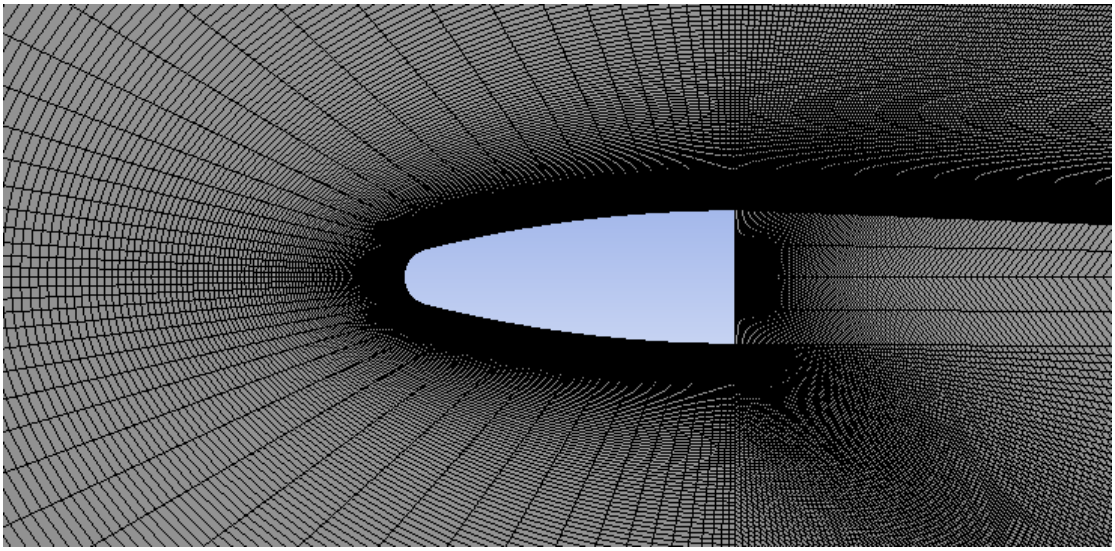

Fig. 3. Mesh generation of the spherical blunted tangent ogive nose

The computational domain quality will take an important role in the stability and accuracy of the calculation. Thus, to control the mesh quality, a number of criteria can be predicted in Fluent package such as maximum skewness and aspect ratio. The region close to the body nose was needed to greater computational accuracy [15].

After completing the meshing of model, it was applying ANSYS Fluent 17.0 and the parameter for the simulation was established. Density based approach is used as it the most preferred compressible high-speed flows. The $k-\omega$ turbulence models were used given its suitability for modeling flows separated regions. A pressure far-filled boundary condition allows the user to specify Mach number, static pressure, static temperature and turbulent condition for the flow at the free stream flow locations. The model type solver pressure based with viscous model as Spalart-Allmaras. Ideal gas law to determine the air density, while Sutherland's was used to calculate the air viscosity. The turbulence intensity was set to 1% with turbulence length scale being the same as the body nose.

4.1 Dynamic Mesh

The difficulty in simulating moving geometry and fluid structure interaction (FSI) applications using traditional techniques is mainly due to the limitation and restriction imposed by the underlying computational mesh. The option of dynamic mesh is adopted during each transient simulation to get high mesh quality and prevent formation of negative cell volumes due to deterioration of mesh quality. In Ansys Fluent the dynamic mesh capability is used to simulated problem with boundary motion, such as moving wall (body nose). In the current study, the boundary motion is described by a UDF (User Define Function) [13, 16]. A UDF is a function written in scheme of C-programing language which can be dynamically linked with the Fluent. UDF's are executed as either interpreted or compiled function in Fluent. The UDF code defines the mesh motion through dynamic zones, which correspond to the centre of gravity motion of moving body nose. For simple dynamic mesh problems involving linear boundary motion and the spring-based smoothing was used to update the volume mesh in the deforming zones.

4.2 Grid Independency Study

In order to determine the results sensitivity to grid refinement, seven different grids have been employed and tested the temperature for conical nose with Mach number 2 at angle of attack 25°. As the number of cell increase, the value for temperature increase until reach to approximately constant value as shown in Figure 4.

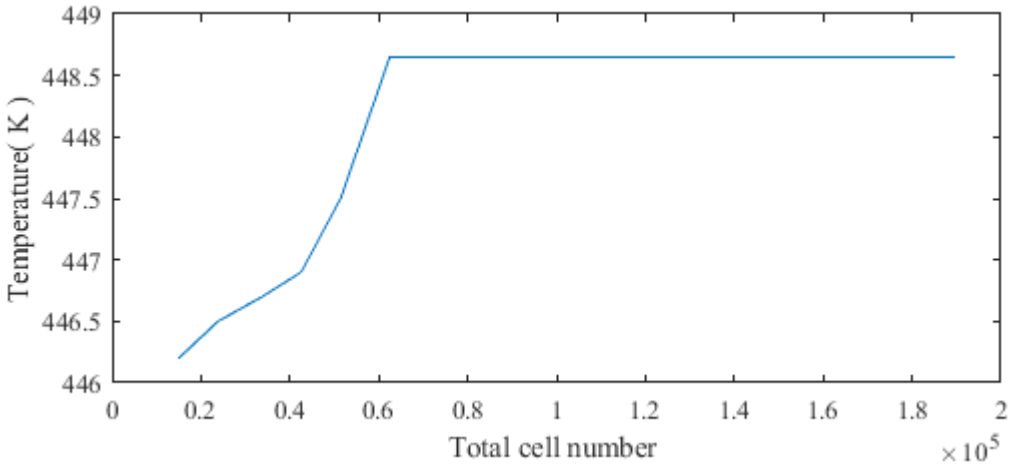

Fig. 4. Grid independency study for temperature at angle of attack 25°

5. Results and Discussion

In order to analyse the results from the different body nose configuration, similar dimension, material and properties, the internal heat and wall temperature over the surface of a body nose was calculated. A numerical solution of 2-D inviscid flow field around the body nose with spherical blunted radius ($r_n = 86mm$) for two noses was carried out by ANSYS program. The effect of altitude has been taken into consideration as well as the variation of properties with time and temperature. All results at altitude $6\ Km$ air pressure 0.46 bars and air temperature $250\ k.^{\circ}$

Due to a fast flying bodies, shock wave generates ahead of the body. The temperature contour is observed from Figure 5 which gets changes drastically across the shock waves. Contours of temperature distribution show that the lower and upper surface of the body nose having equal temperature at zero attack angle. The temperature indicates a large variation in the shock, especially

near the solid wall. Furthermore, most of kinetic energy converts into internal energy crossing the shock wave.

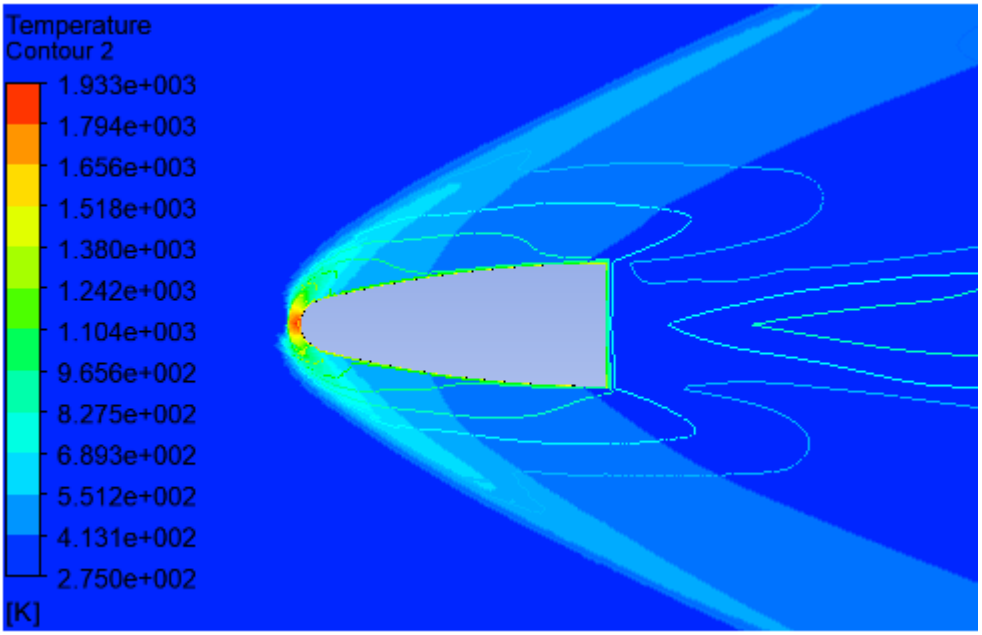

Fig. 5. Temperature contour at zero attack angle for ogive nose at Ma=5

From the results simulation it is obtained at Mach number 5 with zero attack angle as shown in Figure 6 to 9. The friction of the fluid flow around the body nose and on the flow, compression occurs near stagnation point. The heating under consideration consists of convection from the boundary layer on the surface of the body nose and conduction inside the structure. Another important point in these figures, it is quite clear that as the maximum temperature occurs at the tip of nose body (stagnation point) where the flow is usually decelerated and brings it down to zero velocity but the temperature and heat for a conical nose is higher than for the ogive and about 3 %.

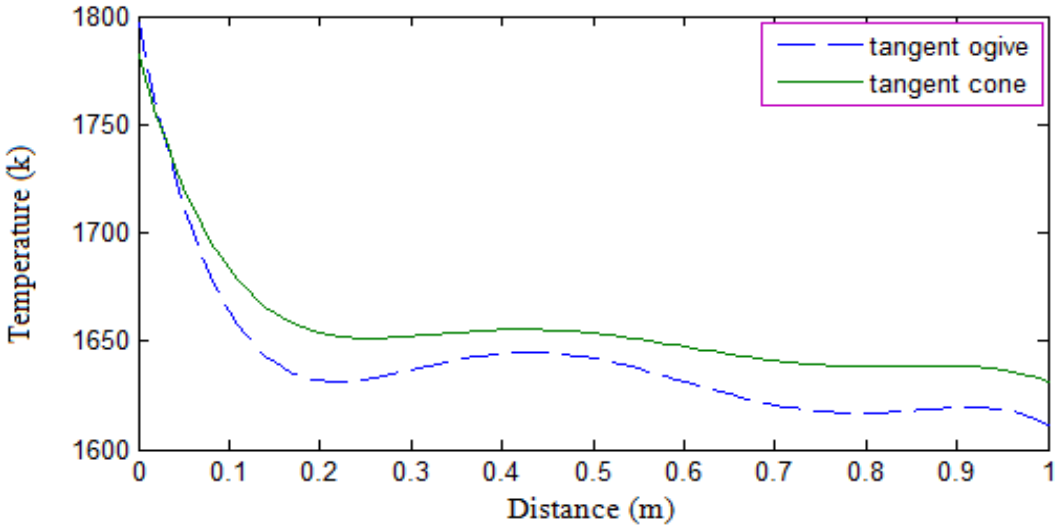

Fig. 6. Temperature distribution over the body nose at zero attack angle

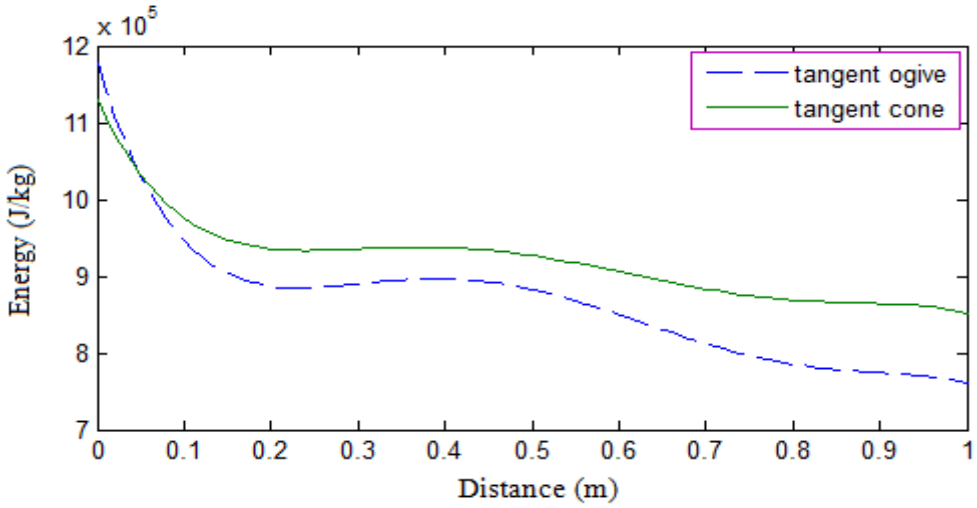

Fig. 7. Energy variation along body nose at zero attack angle

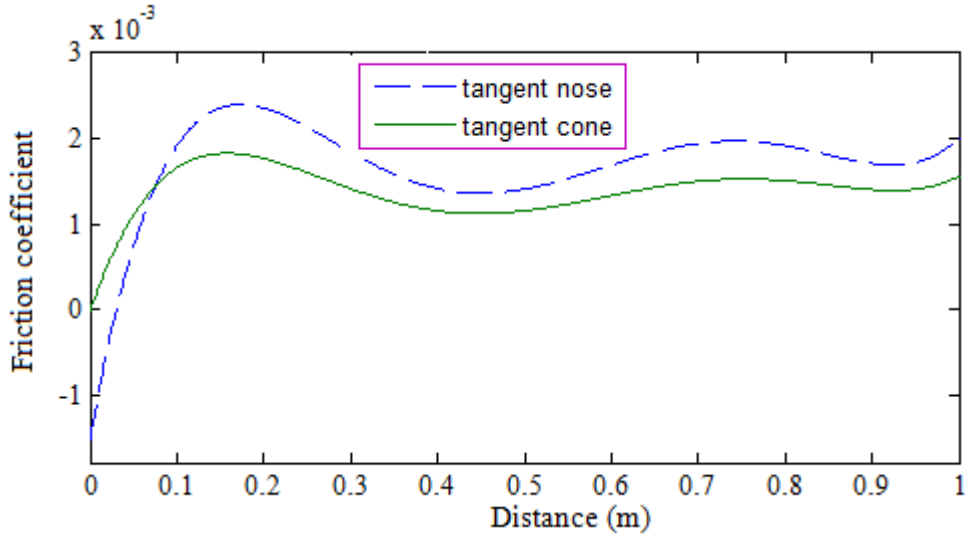

Fig. 8. Friction coefficient variation along body nose at zero attack angle

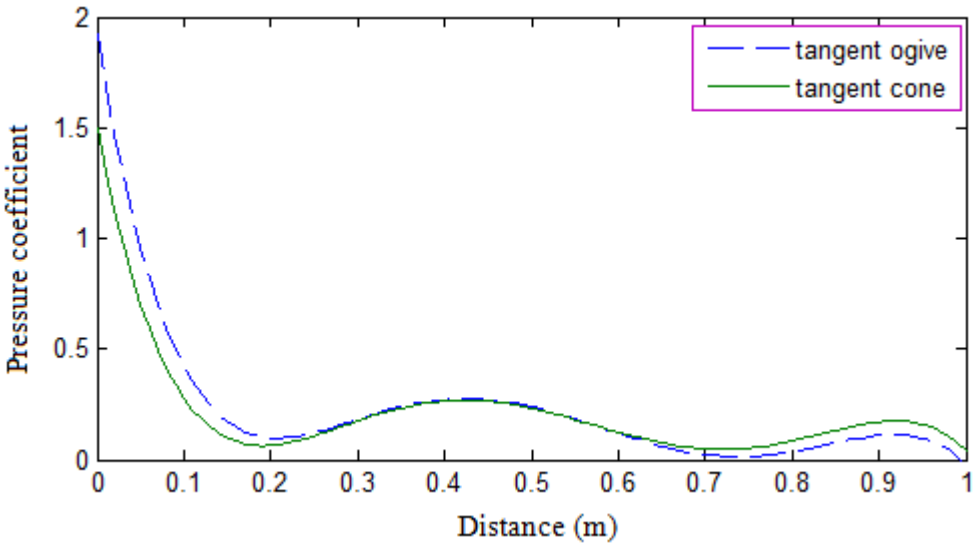

Fig. 9. Pressure coefficient variation along body nose at zero attack angle

It can be seen from Figure 10 to 13, the effect of increasing attack angle on the internal heat and temperature, it was examined. From the figures it is observed that; the angle of attack has a direct impact on the internal heat and temperature, but this increase depends on the body nose configuration, as they have different effects on its performance in flight. Also, the different temperatures between them increase with attack angle.

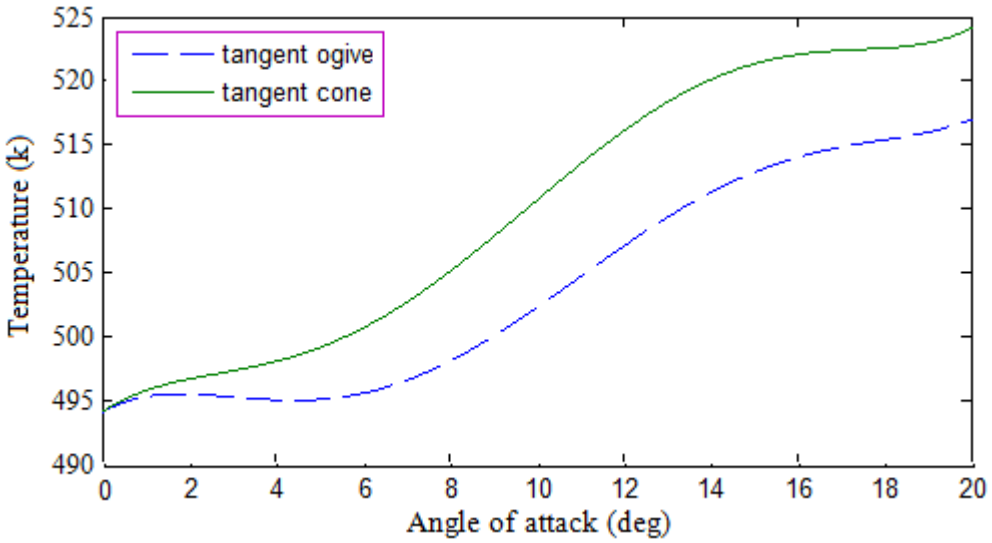

Fig. 10. Wall temperature variation with attack angle at Ma=2

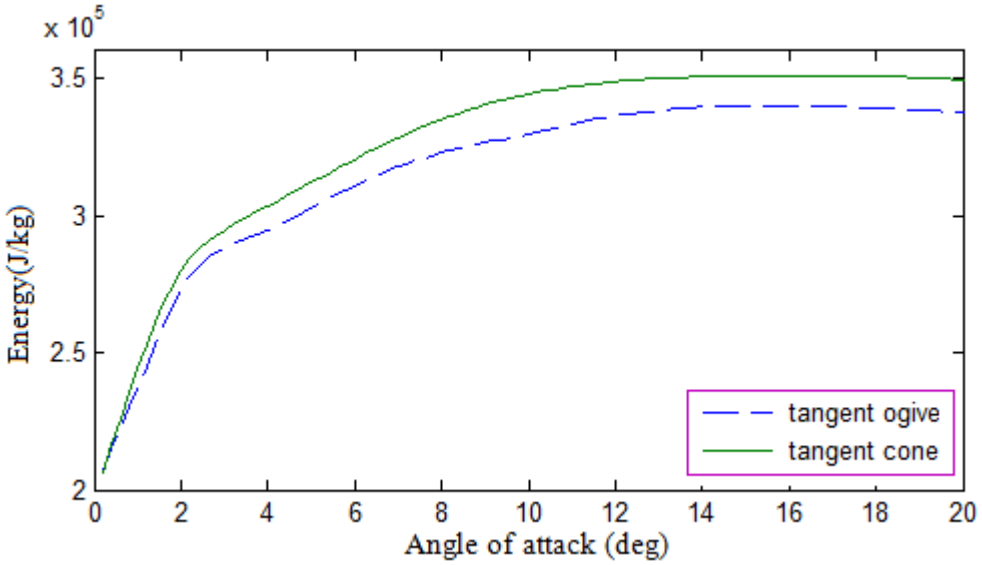

Fig. 11. Internal energy variation with attack angle at Ma=2

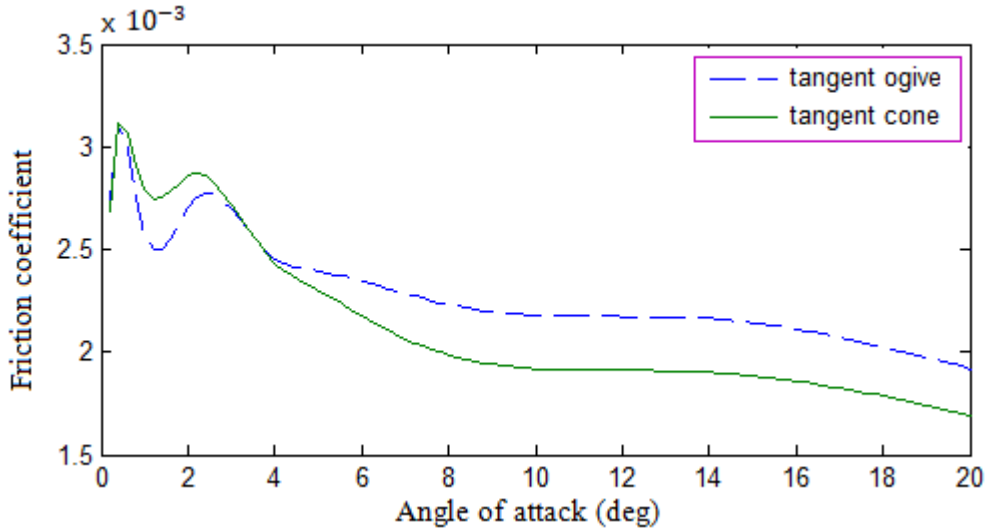

Fig. 12. Friction coefficient variation with attack angle at Ma=2

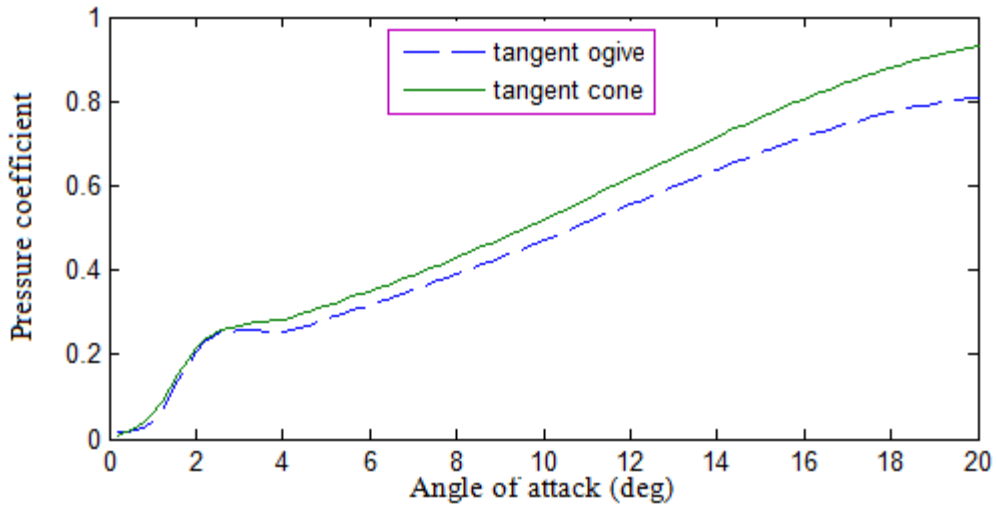

Fig. 13. Pressure coefficient variation with attack angle at Ma=2

From the temperature contour shown in Figure 14 we show that, when the attack angle increases the temperature of lower surface was much higher than the temperature of the upper surface. Due to the large surface of the body nose comes in contact with fluid and this lead to the thermal increase in the body nose surface then causes an increase in the body thermal stresses which is the main cause of mechanical failure and must be taken in design of body nose.

The aerodynamic heat of hypersonic flight in different Mach numbers is simulated through flow field analysis. The variation of temperature and heat with respect to Mach number as shown in Figure 15 and 16, respectively.

As the Mach number increases, flow disturbances will occur and may be the starting point for greatest streamlined bodies. The result predicts the internal heating and wall temperature to be proportionally increased with increases of the Mach number; Temperature and heating become critical, to avoid overheating, the simplest method is to be flying at higher altitudes (lower air densities and temperature).

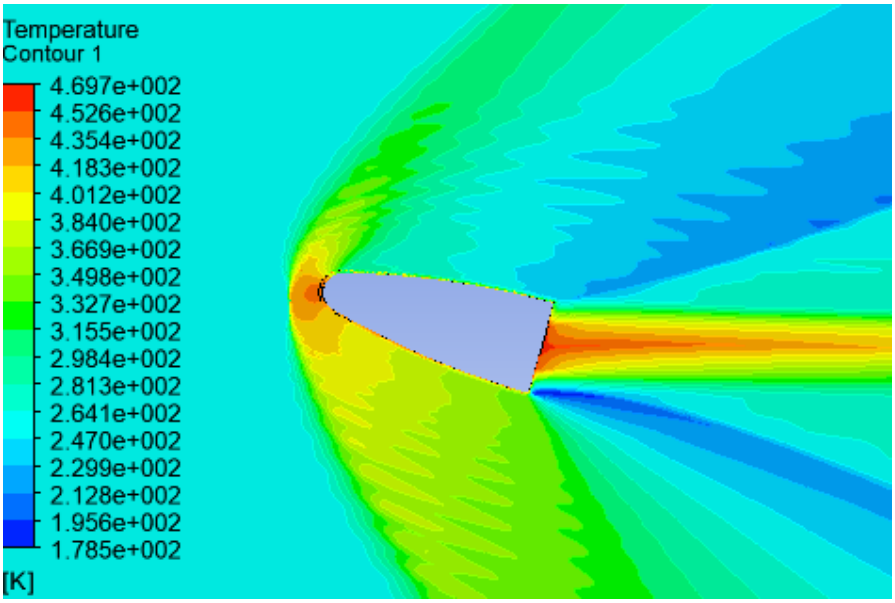

Fig. 14. Temperature contour for ogive nose at high attack angle and Ma=2

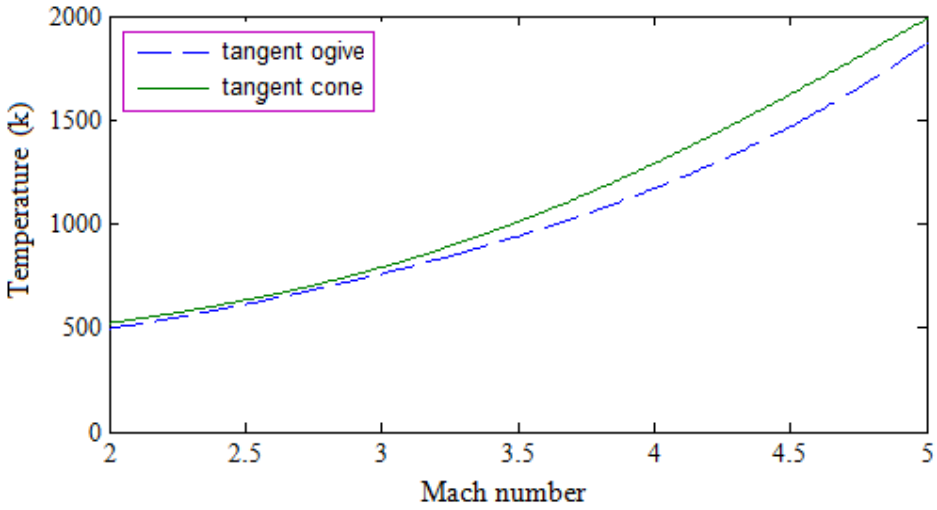

Fig. 15. Variation of temperature with respect to Mach number at zero attack angle

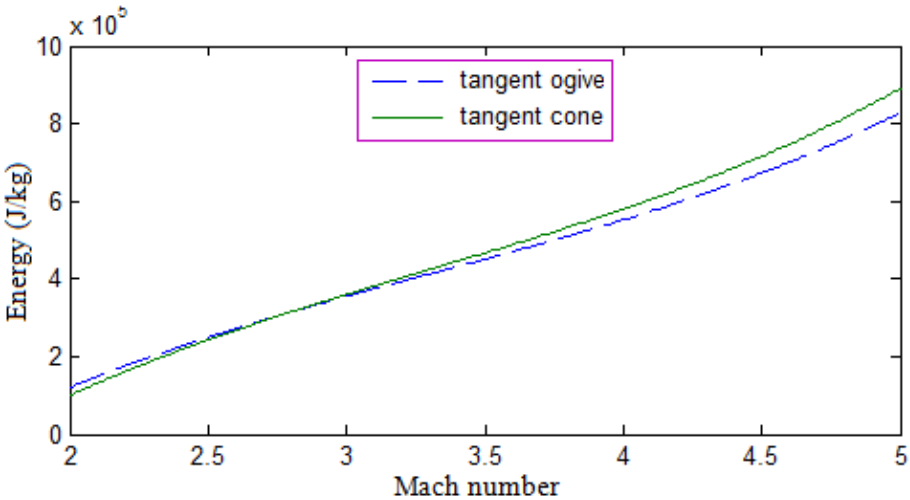

Fig. 16. Variation of energy with respect to Mach number at zero attack angle

For validation of the present work, the heat distribution of temperature over the conical nose with respect to Mach number at zero attack angle are verified with the theoretical calculations in Davles and Monaghan [17] as shown in Figure 17 and 18. The results shows that CFD simulation are able to predict wall temperature with an average deviation about 5 % from the analytical result. It is concluded that CFD has the potential of accurately predicting.

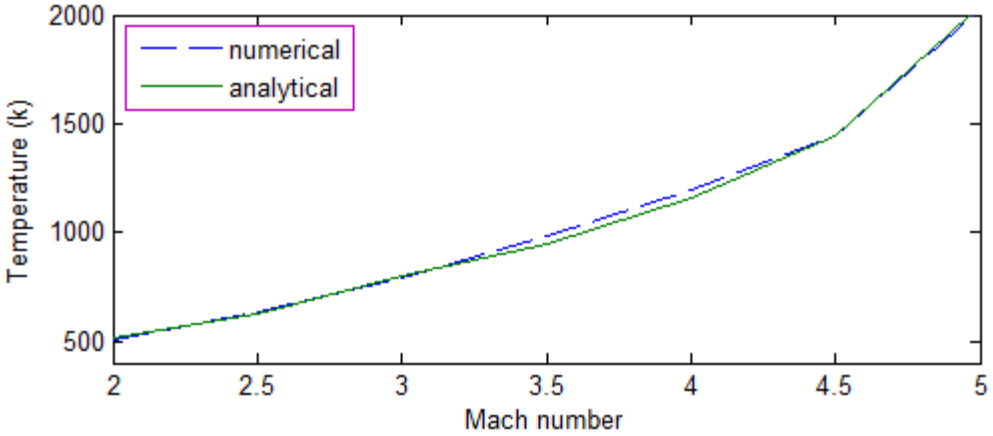

Fig. 17. Variation of temperature with respect to Mach number for two methods [17]

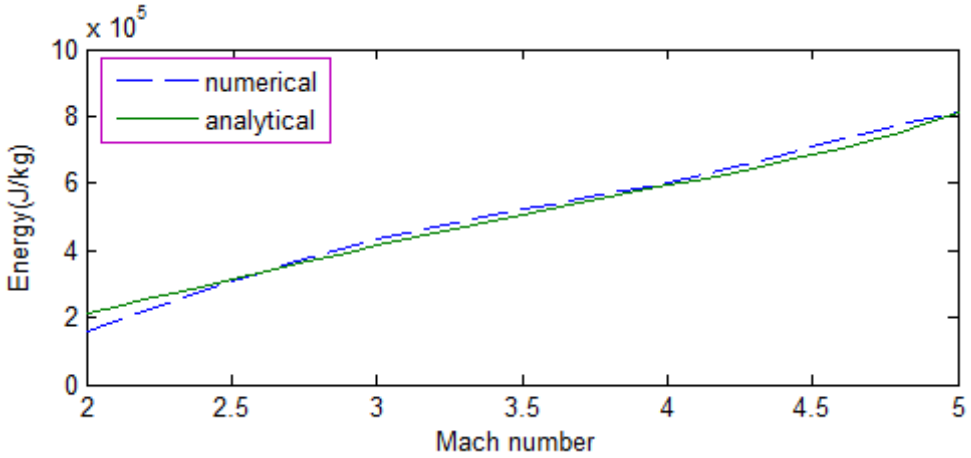

Fig. 18. Variation of energy with respect to Mach number for two methods [17]

6. Conclusions

In this work, an improved procedure for predicting heat distribution of temperature on the body nose configuration. The numerical simulations were performed in Fluent CFD to investigate the effects of varied parameters. Dynamic mesh must be used to simulate the motion of the body nose and the following conclusions can be drawn from the above analysis.

i. The analysis of computation results shows that need to use additional thermal protection of the structure part of the body nose. This procedure is useful both in the design of body nose from the thermal stresses point of view as well as the effect of temperature increases in the inner surface upon the equipment installed in it.

ii. In all cases the heat distribution of temperature for a conical nose is higher than for the ogive nose. Moreover, the different between them is increased with increasing the Mach number and angle of attack.

iii. The result show that, the angle of attack has a direct impact on the internal heat and temperature of the boy nose configuration for all Mach numbers

References

[1] Papadopoulou, Ermioni. *Numerical Simulations of the Apollo 4 Re-entry Trajectory*. No. STUDENT. 2014.
[2] COAKLEY, THOMAS. "Numerical simulation of viscous transonic airfoil flows." In *25th AIAA Aerospace Sciences Meeting*, p. 416. 1987.
[3] Harris, Charles D. "Two-dimensional aerodynamic characteristics of the NACA 0012 airfoil in the Langley 8 foot transonic pressure tunnel." (1981).
[4] Alex J. Schneider. "Computational Modelling of Total Temperature Probes." (Master Thesis, Blacksburg, Virginia, 2015).
[5] Alberto Ferrero. "Calculation and Optimization of Aerodynamic Coefficients for Launchers and Re-Entry Vehicles." (Master thesis, Instituto Superior Técnico, University of Lisbon, Portugal, 2014).
[6] Allen, H. Julian, and Alfred J. Eggers Jr. "A study of the motion and aerodynamic heating of missiles entering the earth's atmosphere at high supersonic speeds." (1953).
[7] Chauvin, Leo T. "Aerodynamic heating of aircraft components." (1956).
[8] Nassir, Sheikh Abdul Hadi, Fazila Mohd Zawawi, Mohamad Zahid Mazlan, Syahrullail Samion, Muhammad Afiq Witri Muhammad Yazid, and Ummikalsom Abidin. "Numerical Investigation of Wake Energy Induced by Cruising Passenger Vehicles on Highway." *Journal of Advanced Research in Fluid Mechanics and Thermal Sciences* 57, no. 2 (2019): 175-185.
[9] Rozaim, Muhammad Faiz, Fazila Mohd Zawawi, Nur Safwati Mohd Nor, Haslinda Mohamed Kamar, and Nazri Kamsah. "Experimental study on performance of low speed wind turbine for application in Malaysia." *Journal of Advanced Research in Fluid Mechanics and Thermal Sciences* 26, no.1 (2016): 20-28.
[10] Crowell Sr, Gary A. "The descriptive geometry of nose cones." *URL: http://www. myweb. cableone. net/cjcrowell/NCEQN2. doc* (1996).
[11] Boukharouba, Taoufik, Fakher Chaari, Mounir Ben Amar, Krimo Azouaoui, Nourdine Ouali, and Mohamed Haddar. "Computational Methods and Experimental Testing In Mechanical Engineering." (2019).
[12] Aqil, Laeeq Ahmed Khan, GM Sayeed Ahmed, P. Ravinder Reddy, and S. Nawazish Mehdi. "Flow Prediction for Variable Angle of Attack Analyzing Lift And Drag Coefficient of An Aerofoil Subjected to Different Turbulence Effects."
[13] Ansys user's Manual (15.0) "SWANSON ANSYS SYSTEM INC." SASI), (2013).
[14] Kishor Gajanan Malokar, and Narendra R. Deore. "Numerical Simulation of Uneven Heating of Missile Surface Travelling at Supersonic Speed." *International Engineering Research Journal* (2016): 699-709.
[15] Duarte, G., M. Silva, and B. M. Castro. "Aerodynamic Heating of Missile/Rocket-Conceptual Design Phase." In *Proceeding of COBEM 2009, 20th International Congress of Mechanical Engineering*. 2009.
[16] Pradev D., Suchith K. "Theoretical Analysis of Influence of Attack Angle on Coefficient of Drag of a Re-Entry Vehicle Using CFD Tools." *World Journal of Engineering Research and Technology* 2, no. 5 (2016): 174-180.
[17] Davies, F. V., and R. J. Monaghan. *The Determination of Skin Temperatures Attained in High Speed Flight*. HM Stationery Office, 1953.